

OPEN ACCESS

Coating of NCM 851005 Cathode Material with $\text{AlO}@\text{Al}_2\text{O}_3$ and Subsequent Treatment with Anhydrous HF

To cite this article: Arthur Martens *et al* 2020 *J. Electrochem. Soc.* **167** 070510

View the [article online](#) for updates and enhancements.



Coating of NCM 851005 Cathode Material with Al⁰@Al₂O₃ and Subsequent Treatment with Anhydrous HF

Arthur Martens,^{1,=} Christoph Bolli,^{2,=} Anke Hoffmann,¹ Christoph Erk,³ Thilo Ludwig,¹ Mario El Kazzi,^{2,*} Ulf Breddemann,¹ Petr Novák,² and Ingo Krossing^{1,z}

¹Institut für Anorganische und Analytische Chemie and Freiburger Materialforschungszentrum (FMF), Universität Freiburg, 79104 Freiburg, Germany

²Paul Scherrer Institute, 5232 Villigen PSI, Switzerland

³BASF SE, 67056 Ludwigshafen, Germany

The volatile alane (H₂AlO'Bu)₂ decomposes into amorphous HAIO or Al⁰@Al₂O₃ nanoparticles upon heating, depending on the time and temperature. By coating the Ni-rich cathode material NCM851005 with this compound, the NCM's cycling stability and electric conductivity were increased. Thus, the coating not only yielded Al⁰@Al₂O₃ nanoparticles but also, by reaction with surface Li₂O/LiOH/Li₂CO₃, a Li⁺ conductive LiAlO₂ layer. The coatings with 0.3 and 0.1 wt% (H₂AlO'Bu)₂, respectively, significantly reduced the resistance build-up to 70/115% after 280 cycles at 1 C (351% without coating). Upon treatment of the 0.3 wt% Al-coating with two equivalents of anhydrous HF, the Al₂O₃ and LiAlO₂ parts were transformed into a Li[AlO(OH)F] layer, which yielded better capacity retention, retaining the low impedance build-up of only +120% (280 cycles at 1 C). This treatment, however, proved to have the same effect as simply reducing the amount of (H₂AlO'Bu)₂ for the coating to 0.1%.

© 2020 The Author(s). Published on behalf of The Electrochemical Society by IOP Publishing Limited. This is an open access article distributed under the terms of the Creative Commons Attribution 4.0 License (CC BY, <http://creativecommons.org/licenses/by/4.0/>), which permits unrestricted reuse of the work in any medium, provided the original work is properly cited. [DOI: 10.1149/1945-7111/ab68d0]



Manuscript submitted November 7, 2019; revised manuscript received December 16, 2019. Published January 20, 2020. *This paper is part of the JES Focus Issue on Challenges in Novel Electrolytes, Organic Materials, and Innovative Chemistries for Batteries in Honor of Michel Armand.*

Supplementary material for this article is available [online](#)

Portable electronic devices play an important role in today's society and the demand for electric vehicles is rising. Most of these devices are powered by lithium-ion batteries (LIBs) that initially used LiCoO₂ as cathode active material (CAM).¹ Due to the high cost of cobalt, efforts are made to replace it by nickel or manganese.^{1–5} Increasing the Ni content leads to an improved specific charge, but also creates new challenges, like cracking of the secondary particles upon cycling or cation mixing.^{6–9} Thus, usually mixed oxides of the general formula Li_{1+a}(Ni_xCo_yMn_{1-x-y})_{1-a}O₂ (NCM) are used to replace LiCoO₂.¹ Here, the current trend in LIB research is to increase the specific charge of the cathode beyond 200 mAh g⁻¹ by increasing the Ni content up to above 80%.⁷ However, upon charging of these Ni-rich NCMs, highly reactive Ni⁴⁺ is formed. This Ni⁴⁺ is able to react with the electrolyte, which subsequently leads to capacity fading. Additionally, these NCMs tend to undergo phase transition from the layered *R-3m* phase to the spinel (*Fd-3m*) or rock salt (*Fm-3m*) phases at high temperatures or high degrees of delithiation, which further decreases the practical specific charge.¹⁰ Both of these problems were shown to be less pronounced when the surface of the NCM was coated, e.g., with Al₂O₃,^{2,11} TiO₂,¹¹ ZrO₂,¹² AlF₃,^{13,14} LiAlO₂,¹⁵ or even metallic Al.¹⁶

The most convenient procedure for the coating of the NCMs is a wet chemical coating process.⁷ However, these coatings often proved to be non-uniform, which can be solved by subsequent annealing at elevated temperatures.² A more homogeneous coating with defined layer thicknesses can be achieved by a more elaborate ALD coating.^{7,17} Although these coatings increase the cycling stability of the NCMs in general, they still have some drawbacks. They often lead to a decreased conductivity of electrons and/or lithium ions, which results in overpotentials and slightly inferior initial specific charges.² In case of the coating with metallic Al, the rather low electric conductivity of the NCM materials is increased.¹⁶

Intrigued by the positive influence of the Al and Al₂O₃ coatings on the cyclability of the NCMs, we set out to coat the Ni-rich Li_{1+x}(Ni_{0.85}Co_{0.10}Mn_{0.05})_{1-x}O₂ cathode material (NCM851005, x ≈

0.01) with Al and Al₂O₃ at the same time by use of (H₂AlO'Bu)₂ (Bu = C(CH₃)₃) as starting material. This compound was shown to decompose into Al⁰@Al₂O₃ core-shell particles (Al⁰ core, Al₂O₃ shell) upon heating to 200 °C–300 °C.^{18–20} By this hybrid coating, we intended to enhance the oxidative stability and the electric conductivity of NCM851005 at the same time. Additionally, this coating is possible by a simple batch process and therefore could be an alternative to the elaborate ALD techniques, while retaining its advantage of uniform coatings. Furthermore, we intended to coat the NCM with an amorphous compound of the sum formula HAIO (or ionic: H⁺Al³⁺O²⁻) and a hitherto unknown three-dimensional structure, which is formed upon mild heating of (H₂AlO'Bu)₂ to 200 °C.^{21,22} Due to its hydridic H⁻ character, this compound itself is rather unsuited as coating material. However, this high reactivity allows for many transformations into other coatings. Here, we transformed the HAIO/Al⁰@Al₂O₃ into a Li[AlO(OH)F] coating by reaction with anhydrous HF gas and investigated its composition and influence on the cyclability of NCM851005.

Experimental

Synthesis of NCM851005 (Li_{1+x}(Ni_{0.85}Co_{0.10}Mn_{0.05})_{1-x}O₂).—A stirred tank reactor was filled with 5 wt% ammonium sulfate aqueous solution and heated to 55 °C. The pH value of the solution was adjusted to a value of 12 by adding aqueous sodium hydroxide solution. A transition metal (TM) sulfate solution was prepared containing Ni, Co and Mn in a molar ratio of 8.5:1.0:0.5 and a total transition metal concentration of 1.7 mol kg⁻¹. A second solution was prepared by mixing an aqueous 25 wt% sodium hydroxide solution and a 25 wt% ammonia solution in a weight ratio of 6:1. The co-precipitation reaction was carried out by simultaneously feeding the transition metal sulfate solution and the aqueous sodium hydroxide solution into the reactor for approx. 2000 min. The pH value was kept at approx. 12 by the separate feed of aqueous sodium hydroxide solution. The mixed transition metal oxyhydroxide precursor was obtained by filtration of the resulting suspension and drying the solid at 120 °C in air. For calcination, the precursor was mixed with LiOH monohydrate with a Li/(TM) molar ratio of 1.03:1. The mixture was heated to 760 °C and kept for 10 hours under a continuous gas flow of 60% oxygen and 40% nitrogen (by

⁼These authors contributed equally to this work.

*Electrochemical Society Member.

^zE-mail: krossing@uni-freiburg.de

volume). After cooling to ambient temperature, the powder was deagglomerated and sieved through a 32 μm mesh to obtain the final NCM851005 cathode active material. The specific surface area of the NCM was determined to be $0.2\text{ m}^2\text{ g}^{-1}$ by BET measurements with a Gemini 2375 instrument from Micromeritics (multipoint mode).

Coating of NCM851005 with $(\text{H}_2\text{AlO}^i\text{Bu})_2$.—In a glove box, NCM851005 (15 g) and $(\text{H}_2\text{AlO}^i\text{Bu})_2$ (45 mg, 0.3 wt%) were weighed into a glass vial, mixed, put in an autoclave and closed. The autoclave was then stored in an oven at 180 °C for 2 h. After reaching room temperature, the autoclave was transferred into a glove box and the sample was removed from the autoclave and ground. For all analyses, the coated NCM was used as obtained by this method, except for electrochemical measurements. Here, the NCM was stored in a drying oven (60 °C) at ambient air for 3 days in order to oxidize all potentially present residual Al–H groups, which would react with the electrolyte. Inductively coupled plasma optical emission spectrometry (ICP-OES) of the coated NCM851005 revealed an Al-content of 0.06 wt%, which is in agreement with the theoretical value of 0.08 wt%. The sample coated with 0.1 wt% was prepared analogously. For NMR and powder XRD experiments the mass of $(\text{H}_2\text{AlO}^i\text{Bu})_2$ was increased to 5 wt% using the same procedure.

Treatment of the coated NCM851005 with aHF gas.—After the initial coating with $(\text{H}_2\text{AlO}^i\text{Bu})_2$ performed as described above, 15 g of the 0.3/0.1 wt% coated NCM were transferred inside a glove box into a PFA (perfluoroalkoxy-polymer) batch reactor, equipped with a stir bar, and closed. The reactor was transferred to a Monel vacuum line with a volume of 74 ml and evacuated. Then the vacuum line was filled with 2 equiv. of gaseous HF (330 mbar) with respect to the HAlO expected, passed into the evacuated batch reactor and filled with N_2 up to a pressure of 1 atm. The NCM was stirred in the HF/ N_2 atmosphere for 1 h at r.t. Afterwards the residual HF was pumped off, the reactor was filled with Ar and transferred to the glove box, where the caked sample was ground and stored. The sample coated with 0.1 wt% was treated analogously.

Electrode preparation.—Electrodes contained 93% CAM, 1.5% carbon black (Super C65, Imerys Graphite & Carbon, Switzerland), 2.5% graphite (SFG6L, Imerys Graphite & Carbon, Switzerland) and 3% binder (Polyvinylidene fluoride Solef 5130, Solvay). Slurries were mixed in N-methyl-2-pyrrolidone (Sigma Aldrich) and cast onto aluminum foil (15 μm thick) by doctor blading at a 110 μm wet thickness. After drying of the electrodes at 80 °C in vacuum overnight, circular 13 mm diameter electrodes were punched, weighed and dried at 120 °C under vacuum overnight before entering in an Ar filled glove box.

Half-cell electrochemical measurements.—Coin-type electrochemical cells were assembled in an argon-filled glovebox. The positive 13 mm diameter electrode (loading of CAM: $11.3 \pm 1.1\text{ mg cm}^{-2}$) was separated from the Li foil counter electrode (serving also as a reference electrode; 0.75 mm thick, Alfa Aesar, United States) by a glass fiber separator (Whatman GF/D). 300 μl of LP47 (1 M LiPF_6 in ethylene carbonate (EC):diethyl carbonate (DEC), 3:7 by weight, BASF SE) was used as the electrolyte. Cells were galvanostatically cycled between 3.0 and 4.3 V at a specific current of 210 mA g^{-1} (for 1 C rate) at 25 °C, using an Astrol (Switzerland) standard battery cyler. Most of the data shown in the discussion were obtained from a single cell. The relevant specific discharge capacities, however, were obtained from an average of two cells.

Full-cell electrochemical measurements.—Coin-type electrochemical cells were assembled in an argon-filled glovebox. The positive 14 mm diameter electrode (average loading of CAM: 10 mg cm^{-2}) was separated from the commercial “potato-shape”

anode graphite negative electrode (average loading 7.1 mg cm^{-2}) by a glass fiber separator (Whatman GF/D). 100 μl of LP572 (1 M LiPF_6 in ethylene carbonate (EC):ethyl methyl carbonate (EMC), 1:1 by weight, containing 2 wt% vinylene carbonate, BASF SE) was used as the electrolyte. For each sample a single cell was galvanostatically cycled between 2.7 and 4.2 V at a 1 C rate at 45 °C (to accelerate fading of the cells), using a Maccor 4000 battery cyler.

During the resistance measurement (conducted every 25 cycles at 25 °C), the cell was charged in the same manner as for cycling. Then, the cell was discharged for 30 min at 1 C to reach 50% state of charge. To equilibrate the cell, a 30 s open circuit step followed. Finally, a 2.5 C discharge current was applied for 30 s to measure the resistance. At the end of the current pulse, the cell was again equilibrated for 30 s at open circuit and further discharged at 1 C to 2.7 V vs graphite.

To calculate the resistance, the voltage at open circuit before applying the 2.5 C pulse current, $V_{0,s}$, and after 10 s of 2.5 C pulse current, $V_{10,s}$, as well as the 2.5 C current value, I (in A), were taken. The area-specific resistance was calculated according to Eq. 1 (S: electrode area, V: voltage, I: 2.5 C pulse current).

$$R = \frac{V_{0,s} - V_{10,s}}{I} S \quad [1]$$

Powder XRD measurements (pXRD).—The samples were filled into a capillary with an outside diameter of 0.3 mm with 0.01 mm wall thickness. pXRD data were collected with a Stoe Stadi P powder diffractometer with $\text{Mo-K}\alpha_1$ radiation, a Ge(111) monochromator and a Mythen 1k detector. A LeBail refinement of the lattice parameters was performed with the GSAS program.

MAS NMR measurements.— ^{27}Al and ^{19}F magic angle spinning nuclear magnetic resonance experiments were performed on a Bruker DSX 500 solid-state NMR spectrometer running at a Larmor frequency of 130.34 MHz and 470.65 MHz for ^{27}Al and ^{19}F , respectively. The rotor synchronized Hahn Echo experiments were performed at magic angle spinning rates of 25 kHz to 33.3 kHz using a 2.5 mm MAS probe with an $\omega_1/2\pi$ frequency of 125 kHz (i.e. a 90° pulse duration of 2 μs). The MAS spectra were detected with relaxation delays of 2 s (^{27}Al) and 20 s (^{19}F). All spectra were measured at r.t, leading to sample temperatures of 300–325 K, due to frictional heating of the magic-angle spinning device.

STEM/EDX measurements.—The sample material for STEM was embedded in Epofix (Struers GmbH, Willich, Germany) and cut by ultramicrotomy with a thickness of approximately 350 nm. The sample was imaged by TEM using a Tecnai Osiris machine (FEI Company, Hillsboro, USA) operated at 200 keV under high-angle annular dark-field scanning TEM (HAADF-STEM) conditions. Chemical composition maps were acquired by energy-dispersive X-ray spectroscopy (EDXS). Images and elemental maps were evaluated using the iTEM (Olympus, Tokyo, Japan, version: 5.2.3554) as well as the Esprit (Bruker, Billerica, USA, version 1.9) software packages. Microtomy is not able to cut the primary particles of the dense CAM. The secondary particles break along the grain boundaries of the secondary particles. Holes in the cross-sections are a known artifact from the preparation. This was checked by test preparations using focused ion beam milling (FIB).

SEM measurements.—Scanning electron microscopy (SEM) was performed using an Ultra55 machine (Zeiss, Jena, Germany). The samples were prepared on a carbon grid mount and coated with a ~6 nm thick Pt layer by sputtering.

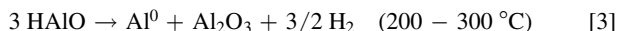
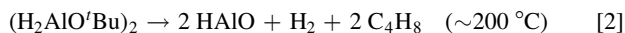
EDX measurements.—EDX elemental analyses (without mapping) were performed using an INCA x-act machine (Oxford Instruments, Oxfordshire, Great Britain) and the results were

analyzed with the software INCA (Oxford Instruments, Oxfordshire, Great Britain). The samples were prepared on a carbon grid mounted on an aluminum sample holder. The analyzed area was about 400 μm^2 .

XPS measurements.—The XPS measurements were conducted with a VG ESCALAB 220iXL spectrometer (Thermo Fisher Scientific) using focused monochromated Al $K\alpha$ radiation (1486.6 eV) with a beam size of $\sim 500 \mu\text{m}^2$ (power of 150 W). The pressure in the analysis chamber was approximately 2×10^{-9} mbar. The spectrometer was calibrated to a clean silver surface by measuring the $\text{Ag}3d_{5/2}$ peak at a binding energy (BE) of 368.25 eV with a full width at half maximum (FWHM) of 0.78 eV. All the spectra were recorded under the conditions of 30 eV pass energy in steps of 50 meV and dwell time of 50 ms. The peaks deconvolution were realized by applying the sum of 70% Gaussian—30% Lorentzian line shapes after Shirley-type background subtraction.

Results and Discussion

Determination of the coating conditions.—Preliminary experiments for the determination of the coating conditions were performed with a similar base cathode material but consisting of NCM811 (synthesis analogous to NCM851005). Prior to the actual coating process, the coating temperature for decomposition of $(\text{H}_2\text{AlO}'\text{Bu})_2$ had to be determined. Pure $(\text{H}_2\text{AlO}'\text{Bu})_2$ decomposes in a two-step procedure according to Eqs 2 and 3:



It was expected that the CAM might (catalytically?) lower the decomposition temperature of the $(\text{H}_2\text{AlO}'\text{Bu})_2$ a bit. Therefore, a large Schlenk tube was loaded with NCM811 on one side and with $(\text{H}_2\text{AlO}'\text{Bu})_2$ on the other side (see electronic supporting information ESI, figure S-1 (available online at stacks.iop.org/JES/167/070510/mmedia). Under a constant Ar flow the $(\text{H}_2\text{AlO}'\text{Bu})_2$ was heated until it started to sublime ($\sim 80^\circ\text{C}$). Then the NCM811 was heated to the same temperature and the temperature was raised step-wise until a white layer formed on top of the CAM. The Schlenk tube was immediately opened and the temperature of the NCM811 was measured. By this method the optimized coating temperature was determined to be 160°C . In order to allow for a complete conversion, we performed all coatings at 180°C .

The actual coating was then performed in an autoclave by mixing 5 to 15 g of the CAM with the desired amount of $(\text{H}_2\text{AlO}'\text{Bu})_2$ in a glass vial and heating it to 180°C . Since the autoclave did not have a pressure relief valve, the pressure raised during the coating procedure due to heating and also due to formation of H_2 and *iso*-butene C_4H_8 (Eq. 2).²¹ Since the increased pressure may inhibit the decomposition of $(\text{H}_2\text{AlO}'\text{Bu})_2$, we determined the weight loss after the coating. Even when using a rather large amount of $(\text{H}_2\text{AlO}'\text{Bu})_2$ (260 mg, 5 wt%), 52% of its weight were gone after the coating procedure. The theoretical mass loss was calculated to be 57% and 58% for the formation of HAIO and $\text{Al}^0/\text{Al}_2\text{O}_3$ (Eqs. 2 and 3). The observed mass loss is in good agreement with the theoretical values, considering weighing errors due to the additional mass of the NCM

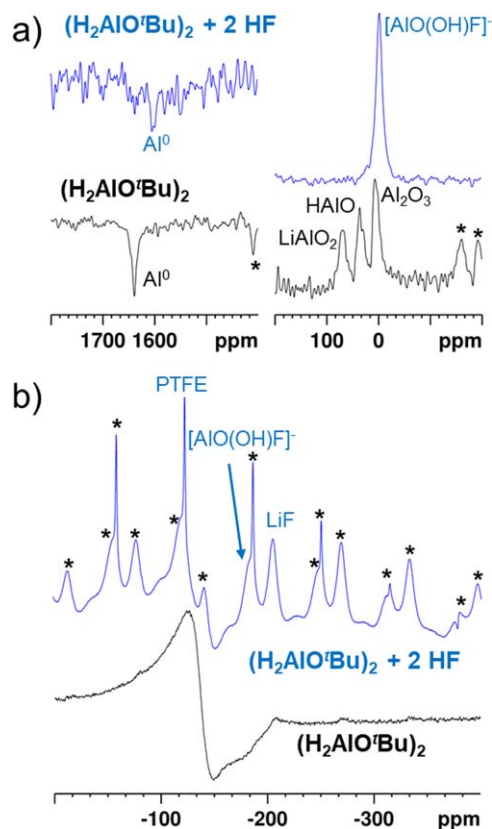


Figure 1. Sections of the MAS NMR spectra of NCM851005 coated with 5 wt% $(\text{H}_2\text{AlO}'\text{Bu})_2$ prior (black) and after treatment with HF gas (blue). Spinning sidebands are marked with an asterisk. Full spectra are shown in the ESI. (a) ^{27}Al NMR spectra, (b) ^{19}F NMR spectra. Treatment of NCM851005 with $(\text{H}_2\text{AlO}'\text{Bu})_2$ for 2 h at 180°C leads to formation of LiAlO_2 , HAIO and $\text{Al}^0/\text{Al}_2\text{O}_3$. Treatment of this coating with HF reduces the amount of Al^0 and the LiAlO_2 , HAIO and Al_2O_3 are transformed into “Li[AlO(OH)F].” Additionally, LiF is formed by reaction with the NCM. The presence of PTFE results from the stir bar used for the HF treatment.

and of the glass flask. Therefore, the formation of the coating was assumed quantitative, even at these elevated pressures. It should be kept in mind that due to the weight loss, using 0.1, 0.3 and 5 wt% $(\text{H}_2\text{AlO}'\text{Bu})_2$ results in a final coating mass of only 0.04, 0.13 and 2.15 wt%, respectively. Yet, we will refer to the initial mass of $(\text{H}_2\text{AlO}'\text{Bu})_2$ used for the coating throughout the entire manuscript. By chance this also corresponds almost exactly to the molar fraction of the coating (1 wt% $(\text{H}_2\text{AlO}'\text{Bu})_2 \hat{=} 1 \text{ mol}\%$ coating, since the average molar masses are about 100 g mol^{-1} (NCM851005) and 102 g mol^{-1} (monomeric unit in dimeric $(\text{H}_2\text{AlO}'\text{Bu})_2$).

Since these initial coatings were applied with heating for 6 h, pXRD traces of the coated NCM811 indicate the diffusion of Al^{3+} into the cathode material due to a slight increase of the cell volume (Table I). Reflexes of new phases could not be found in the pXRD traces (ESI, figure S-2 and S-3). Storing the coated sample at 250°C for another 6 h led to further increase of the cell volume. Therefore,

Table I. Unit cell parameters of NCM811 and NCM851005 from pXRD measurements before and after coating with 5 wt% $(\text{H}_2\text{AlO}'\text{Bu})_2$.

CAM	Coating time/h	<i>a</i> axis/Å	<i>c</i> axis/Å	Ratio <i>cl</i> <i>a</i>	Cell volume/Å ³
NCM811	pristine	2.872088(18)	14.208759(147)	4.9472	101.504(1)
NCM811	6	2.872275(18)	14.209112(149)	4.9470	101.520(1)
NCM811	12 ^{a)}	2.872660(18)	14.210859(152)	4.9469	101.559(1)
NCM851005	pristine	2.871465(22)	14.188216(181)	4.9411	101.313(2)
NCM851005	2	2.872063(24)	14.189569(191)	4.9405	101.365(2)

a) 6 h at 180°C , then 6 h at 250°C .

in order to prevent this Al^{3+} diffusion, the coating time was reduced to 2 h for NCM851005. Under these conditions, the decomposition of $(\text{H}_2\text{AlO}^i\text{Bu})_2$ still proved to be complete, but again was indicative for the diffusion of Al^{3+} into the cathode material (Table I).

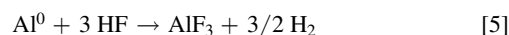
Investigation and Characterization of the Coatings

MAS NMR measurements.—The decomposition of $(\text{H}_2\text{AlO}^i\text{Bu})_2$ at 180 °C should lead to formation of either HAIO or $\text{Al}^0@/\text{Al}_2\text{O}_3$ particles.^{19,20} In order to identify the composition of the coating, we coated NCM851005 with 5 wt% $(\text{H}_2\text{AlO}^i\text{Bu})_2$ and analyzed it by MAS NMR spectroscopy. In the ^{27}Al MAS NMR spectrum four signals can be found at 7, 36, 69 and 1640 ppm (Fig. 1a, ESI Figs. S-4 and S-5 for the full spectra). These signals can be assigned to HAIO (36 ppm),^{20,21} Al_2O_3 (7 ppm),²¹ and metallic Al (1640 ppm),^{20,21,23} while no signals of residual $(\text{H}_2\text{AlO}^i\text{Bu})_2$ were observed. A signal of HAIO could not be found in the ^1H MAS NMR spectra. The signal at 69 ppm in the ^{27}Al MAS NMR spectrum results from LiAlO_2 ,² which seems to be formed as a byproduct. LiAlO_2 was shown to form, when Al_2O_3 coated cathode materials were tempered at 600 °C.² In our case, the formation of LiAlO_2 from the basic surface impurities (LiOH , Li_2O and Li_2CO_3) occurs at much lower temperatures, possibly due to the high reactivity of the used starting materials.

From these NMR spectra, it can be concluded that by treatment of NCM851005 with $(\text{H}_2\text{AlO}^i\text{Bu})_2$ not only an electrically conductive and oxidation stable $\text{Al}^0@/\text{Al}_2\text{O}_3$ coating is formed, but it also consists of Li^+ ion conductive LiAlO_2 .²⁴ The presence of residual HAIO is not desired due to its high reactivity and it can be oxidized by storing the 5 wt% coated NCM851005 in the drying oven at 60 °C for three days. After this oxidation step the sample did

not react with water, while before a heavy reaction was observed. However, it is questionable, if there even is HAIO present in the relevant samples that were tested in half and full cells, since much less $(\text{H}_2\text{AlO}^i\text{Bu})_2$ was used for their coating compared to the samples for the NMR measurements (0.1, 0.3 vs 5 wt%). Although metallic Al also reacts violently with water, here this is prevented by the Al_2O_3 protective layer.¹⁹ Thus, this reaction can be solely attributed to residual HAIO. After several weeks, the MAS NMR sample also showed a smaller signal for HAIO and an increase in Al_2O_3 due to diffusion of oxygen into the sample (ESI, Fig. S-5).

Another way to remove the reactive Al-H sites we investigated was the reaction of the formal “HAIO” with gaseous HF. This way a “FAIO” coating should be obtained (Eq. 4). We note that this procedure may also transform Al^0 into Al-fluorides; here exemplarily AlF_3 was selected as product (Eq. 5). However, also mixed fluorides/oxides may result.



Unexpectedly, after the HF treatment not only the signal of HAIO, but also the one of LiAlO_2 disappeared in the ^{27}Al MAS NMR spectra. Now the signal for metallic Al (1600 ppm) was heavily decreased and a new intense signal at -2.3 ppm was visible (Fig. 1a, ESI Fig. S-8 for the full spectrum). This ^{27}Al chemical shift at -2.3 ppm is in the region of six-coordinate aluminum. Yet, a distinct assignment of this signal cannot be done, as its chemical shift is neither in agreement with fluorinated alumina (~ 10 ppm) nor with AlF_3 (-16 ppm)^{25,26} or $[\text{AlF}_4]^-$ (-5.7 ppm).²⁷ Although this shift is similar to that of $[\text{AlF}_6]^{3-}$ (-2.4 ppm),²⁸ the according signal

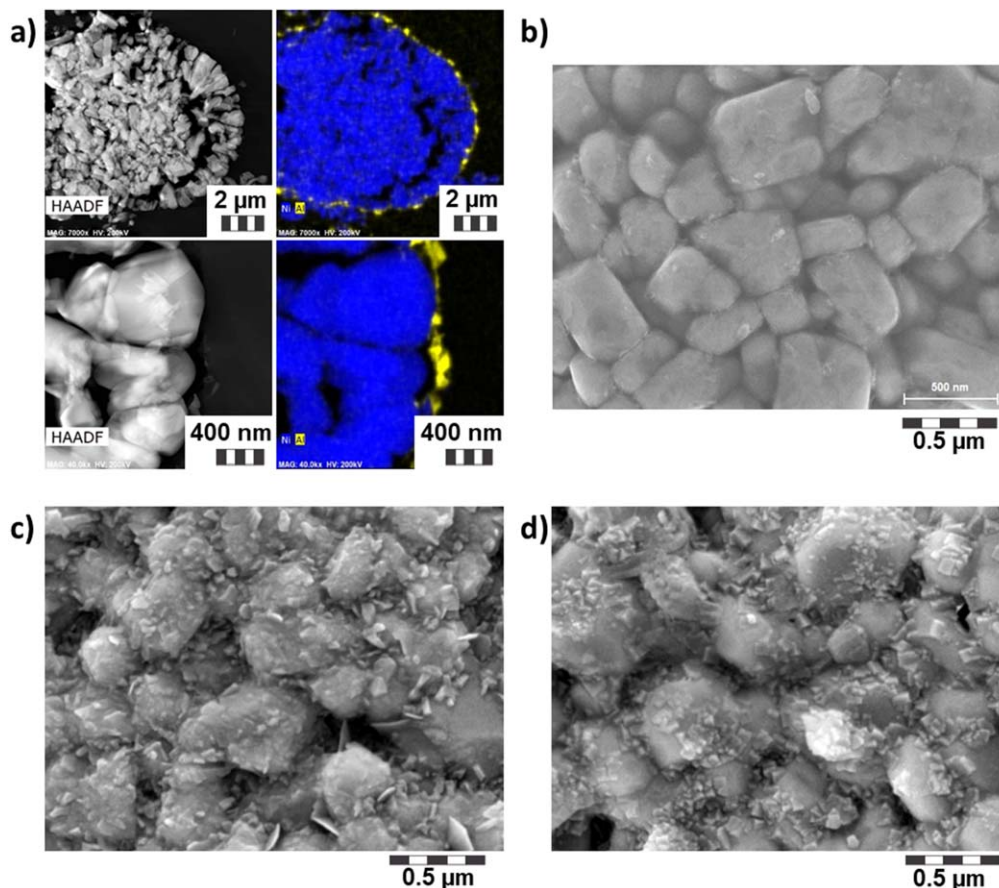


Figure 2. Images of pristine and $(\text{H}_2\text{AlO}^i\text{Bu})_2$ coated (0.3 wt%) NCM851005 before and after HF treatment obtained by TEM and STEM measurements. (a) HAADF-STEM images (left) of the $\text{Al}^0@/\text{Al}_2\text{O}_3$ coated NCM851005 with EDX elemental mapping (right). Scheme: Al (yellow), Ni (blue). (b) SEM image of pristine NCM851005. (c) SEM image of $\text{Al}^0@/\text{Al}_2\text{O}_3$ coated NCM851005. (d) SEM image of $\text{Al}^0@/\text{Al}_2\text{O}_3$ coated NCM851005 after HF treatment.

in the ^{19}F NMR spectrum is expected at a chemical shift of -190 ppm.²⁹ For the discussed sample, a signal at -183 ppm is found in the ^{19}F NMR spectrum and, therefore, the formation of $[\text{AlF}_6]^{3-}$ seems unlikely (Fig. 1b, ESI Figs. S-6 and S-7). As signals of neutral fluorinated alumina are expected in the region between -110 and -165 ppm^{25,26} and anionic aluminum fluorides are usually found at -180 to -200 ppm³⁰ in the ^{19}F NMR spectra, we propose that an anionic fluoro aluminate was formed. Since the chemical shift of this aluminate in the ^{27}Al NMR spectrum is between the ones of LiAlO_2 and $[\text{AlF}_6]^{3-}$, the formed fluoro aluminate probably also contains oxygen atoms. Possible species that could have formed, would be the hitherto unknown $[\text{AlO}(\text{OH})\text{F}]^-$ or $[\text{AlOF}_2]^-$. Additionally to the signals of these proposed anions, also a signal of LiF can be found at -204 ppm in the ^{19}F NMR spectrum, which may enhance Li^+ ion conductivity. The formation of LiF leads to a higher concentration of Li at the NCM's surface, which is extracted from the NCM (see ESI for ^7Li NMR spectra). Considering the reaction stoichiometry of 2:1 (F:Al) and the similar intensities of the signals of LiF and the fluoroaluminate, the formed fluoroaluminate seems to be best described by as $[\text{AlO}(\text{OH})\text{F}]^-$, although it also might be a mixture of (alternating) $[\text{AlO}_2]^-$ and $[\text{AlOF}_2]^-$ or similar structural units. A signal of Al_2O_3 cannot be found in the ^{27}Al NMR spectra but it may be overlapped by the main signal. Yet, the smaller signal of Al^0 provides evidence for its reaction with HF (Eq. 5). It was shown that the Al_2O_3 layer of the $\text{Al}^0/\text{Al}_2\text{O}_3$ particles protects the Al^0 from reaction with gases,¹⁹ hence the Al_2O_3 must have also reacted with the HF (see comprehensive discussion below).

Unfortunately, the characterization of the different coatings by diffuse reflectance infrared Fourier transform spectroscopy (DRIFTS) was not possible due to the high absorbance of the NCM851005, even in KBr mixtures containing only 1% of NCM851005.

Microscopy.—With high-angle annular dark-field STEM (HAADF-STEM, Fig. 2a) images of thin sections of the 0.3 wt% $\text{Al}^0/\text{Al}_2\text{O}_3$ coated NCM851005, the homogeneity of the coating could be investigated. These measurements reveal a thin coating of the NCM with an inhomogeneous distribution of larger particles. The average thickness of the thin layer was determined to be around 30 nm, while the larger particles show a thickness of up to 130 nm. However, XPS measurements (see below) show the presence of Ni at the coated NCM's surface, thus suggesting inhomogeneities even in the thin layer. Additionally, the theoretical thickness of a homogeneous coating using $(\text{H}_2\text{AlO}^i\text{Bu})_2$ was calculated to lead to a layer thickness of 0.9 nm (0.1 wt%) or 2.6 nm (0.3 wt%). Accordingly, the coating has to be inhomogeneous, but appears to reach the chemically reactive places on the CAM due to the gas phase reaction. Since $(\text{H}_2\text{AlO}^i\text{Bu})_2$ is known to form ball-shaped $\text{Al}^0/\text{Al}_2\text{O}_3$ particles at low decomposition temperatures,¹⁹ we

believe that these larger particles mainly consist of $\text{Al}^0/\text{Al}_2\text{O}_3$. The formation of the observed LiAlO_2 requires presence of Li^+ , which is known to be located as Li_2O , LiOH or Li_2CO_3 at the surface of the cathode material. Therefore, it is likely that the thin coating layer mainly consists of LiAlO_2 . The distribution of the residual HAIO cannot be discussed from the available information, if it is existent at all, as discussed before.

This inhomogeneity of the $\text{Al}^0/\text{Al}_2\text{O}_3$ coating can also be seen from scanning electron microscopy (SEM) images (Figs. 2b–2d) and from BET measurements. The SEM images show many small particles on the surface of the NCM's primary particles after the initial coating with $(\text{H}_2\text{AlO}^i\text{Bu})_2$. Consequently, the surface area of the $\text{Al}^0/\text{Al}_2\text{O}_3$ coated NCM851005 is increased to $3.0 \text{ m}^2 \text{ g}^{-1}$ (vs $0.2 \text{ m}^2 \text{ g}^{-1}$ for the pristine material). By treatment of this coating with anhydrous HF , the number of particles and the BET surface ($0.5 \text{ m}^2 \text{ g}^{-1}$) are reduced again due to chemical etching of the $\text{Al}^0/\text{Al}_2\text{O}_3$ particles.

XPS measurements.—X-ray photoelectron spectroscopy was performed on uncycled electrodes of uncoated and both coated (0.3 wt% $(\text{H}_2\text{AlO}^i\text{Bu})_2$ and 0.3 wt% $(\text{H}_2\text{AlO}^i\text{Bu})_2 + 2\text{HF}$) NCM851005 samples. Figure 3 shows the spectra for the $\text{Al}2\text{p}$, $\text{Ni}3\text{p}$ and $\text{Li}1\text{s}$ core levels as well as the deconvolution for the $\text{F}1\text{s}$ core level spectra.

The intensity decrease of the $\text{Ni}3\text{p}$ and $\text{Li}1\text{s}$ peaks confirm the presence of an inhomogeneous coating layer on the CAM particles. Additionally, an $\text{Al}2\text{p}$ peak was observed for the electrodes prepared with the coated NCM851005 samples. The binding energy for the $\text{Al}2\text{p}$ peak for $(\text{H}_2\text{AlO}^i\text{Bu})_2$ coated NCM851005 (74.5 eV) is in agreement with Al_2O_3 ,³¹ thus confirming the observations made by MAS NMR measurements in the previous section. Since no signal of Al^0 is visible in these spectra, the Al_2O_3 layer thickness can be assumed to be higher than 7 nm (penetration depth of XPS). Treatment of the coating with HF leads to a 0.4 eV shift of the $\text{Al}2\text{p}$ peak to higher binding energies (74.9 eV), which confirms the presence of fluoride in the coordination sphere of the aluminum and thus supporting the proposed formation of a fluoroaluminate on the surface as discussed above. Additionally, the formation of AlF_3 and $[\text{AlF}_6]^{3-}$ can definitely be excluded, as their $\text{Al}2\text{p}$ peaks would be expected at 76.3 and 78.7 eV, respectively.^{31,32}

In the $\text{F}1\text{s}$ core level spectrum of the pristine NCM851005 two peaks can be easily distinguished, one can be assigned to C-F from the PVDF binder (687.6 eV), the other to LiF (684.7 eV). LiF is formed as result of a dehydrofluorination of the PVDF binder during preparation of the electrode slurry.^{33,34} This reaction occurs in presence of Brønsted bases in the NMP solution (e.g. residual LiOH) and could eventually lead to gelation of the slurry.^{35,36} For the $(\text{H}_2\text{AlO}^i\text{Bu})_2$ coated sample, both with and without HF treatment, the ratio between the peak areas assigned to LiF and PVDF is

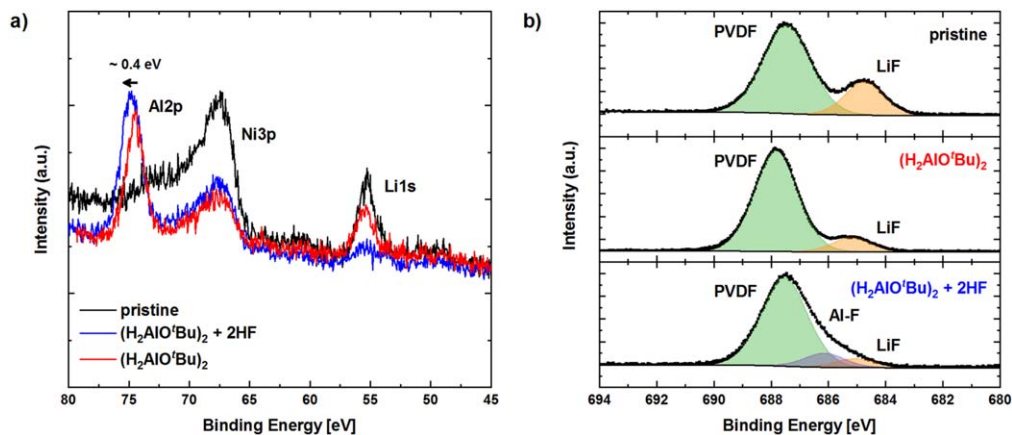


Figure 3. $\text{Al}2\text{p}$, $\text{Ni}3\text{p}$ and $\text{Li}1\text{s}$ (a) and $\text{F}1\text{s}$ (b) core level spectra for uncycled electrodes of pristine NCM851005 and NCM851005 coated with $(\text{H}_2\text{AlO}^i\text{Bu})_2$ or $(\text{H}_2\text{AlO}^i\text{Bu})_2 + 2\text{HF}$. Deconvolution of the $\text{F}1\text{s}$ core level spectra shows the assignment of the PVDF (green), LiF (orange) and Al-F (purple) species.

decreased compared to the pristine sample, indicating the presence of less LiF on the electrodes prepared with the coated NCM851005. Please note that the intensity of the F1s peak assigned to LiF is decreasing in parallel with the Li1s peak intensity, showing that most of the Li detected results from LiF. The decrease of LiF indicates that the applied coating effectively reduces the amount of basic surface residues that are responsible for the dehydrofluorination of the PVDF binder.

For the $(\text{H}_2\text{AlO}^t\text{Bu})_2$ coated sample with HF treatment, the deconvolution of the F1s peak also shows an additional component at 686.2 eV, which can be assigned to a fluoride binding to aluminum. In fact, LiF is hardly detectable for this sample, thus allowing the conclusion that HF is mainly reacting with Al from the surface coating and not with the CAM.

Half-cell cycling of the coated NCM cathode materials.—For testing the cycling performance of the coated NCM851005 samples, five initial activation cycles at C/10 rate were performed first. Then, a rate test with variable discharge rates of up to 5 C (with every charging step at C/2) followed and finally the long term cycling at 1 C (Fig. 4a). The initial specific charge during the activation steps (5th cycle) was around 210 mAh g^{-1} for the pristine material whereas the $(\text{H}_2\text{AlO}^t\text{Bu})_2$ (0.3 wt%) coated NCM851005 showed a roughly 8% lower specific charge (194 mAh g^{-1}). HF treatment of the $(\text{H}_2\text{AlO}^t\text{Bu})_2$ coating reduces the charge loss and with 203 mAh g^{-1} the initial specific charge is only slightly lower than that of the

pristine material. From the normalized charge and discharge profiles in the 5th cycle (Fig. 4b) it can be seen that the $(\text{H}_2\text{AlO}^t\text{Bu})_2$ coated NCM851005 (0.3 wt%) has slightly higher overpotentials during charge and discharge, which is the main cause for the lowered practical specific charge and most likely a consequence of an increased surface resistance due to the coating layer. Treatment of the coating with HF lowers this resistance, reduces the overpotentials, and leads to the aforementioned higher practical specific charge. The coated materials keep their lower specific charge compared to the pristine material during the rate test up to 3 C, only for discharging at 5 C the influence of the additional resistance from the coating is negligible and all three materials achieve the same practical specific charge.

During the long term cycling (Fig. 4c), a constant fading of the pristine material is observed resulting in generally lower coulombic efficiencies and a capacity retention of only 71% after 125 cycles. The $(\text{H}_2\text{AlO}^t\text{Bu})_2$ coated NCM851005 (0.3 wt%) shows a better coulombic efficiency and higher capacity retention (74%). The fluorinated coating shows even better capacity retention (79%), thus its specific charge after 125 cycles (161 mAh g^{-1}) is significantly higher than that of the pristine material (150 mAh g^{-1}). Furthermore, the normalized curves of the specific charge after the long term cycling reveal much higher overpotentials for the pristine material than for the coated materials, of which the fluorinated one again shows a better performance (Fig. 4d). This observation goes in hand with the average voltages during charge/

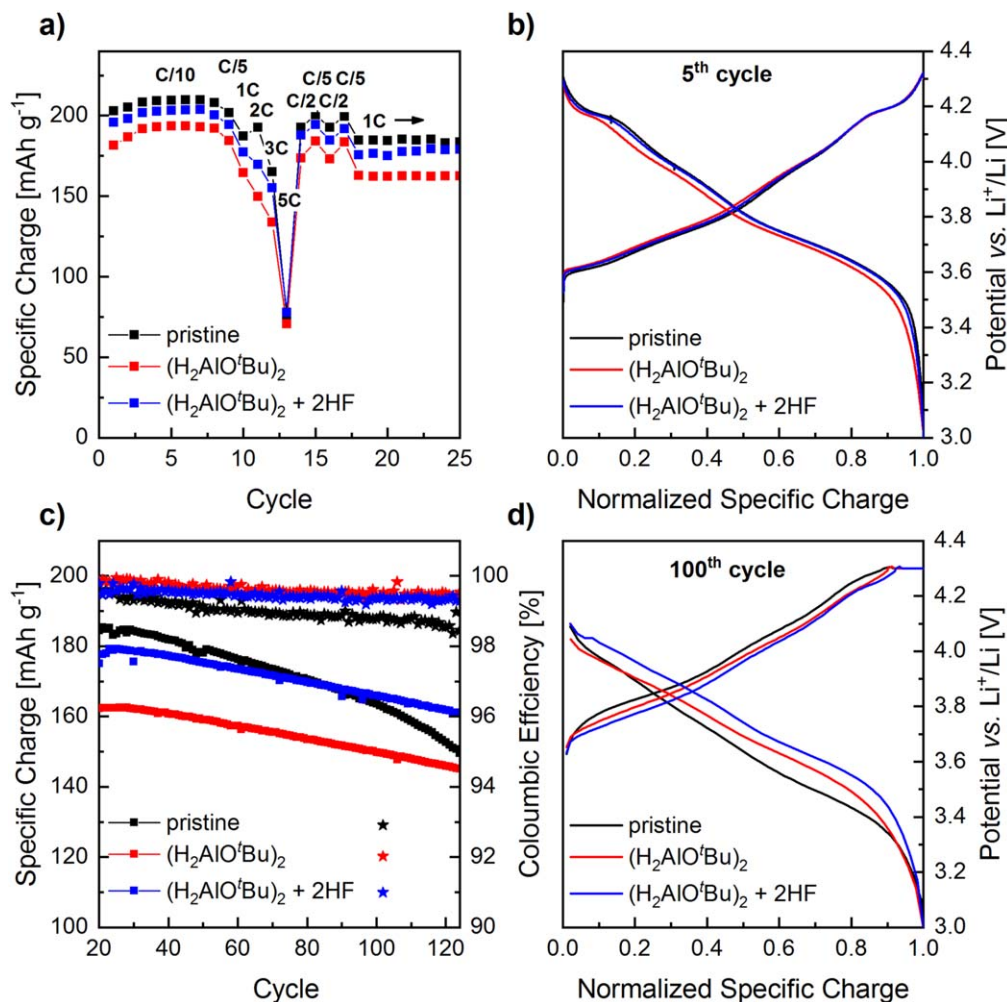


Figure 4. Half-cell cycling data of the pristine (black) and coated NCM851005 prior (red) and after treatment with HF (blue) at 25 °C vs Li using LP47 electrolyte. The first 20 rate-test cycles were performed at various cycling rates shown in fig. (a). Long term cycling was performed at 1 C rate. (a) Specific charge during rate test, (b) normalized specific charge for the 5th cycle, (c) specific discharge capacity during the long term cycling, average of 2 half-cells, (d) normalized specific charge for the 100th cycle. The coating was performed using 0.3 wt% $(\text{H}_2\text{AlO}^t\text{Bu})_2$.

discharge, which show the strongest change for the pristine material (see ESI).

Investigating the influence of the lithium anode.—Interestingly, apart from the absolute values of specific charge, both coated NCM851005 samples show similar cycling stabilities in half-cells, while the pristine NCM851005 shows an inferior cycling stability. In order to evaluate the reason for these differences, in particular the possible influence of the Li counter electrode, we performed another half-cell cycling run of the pristine NCM851005 and of the $(\text{H}_2\text{AlO}^i\text{Bu})_2/\text{HF}$ treated material. After 100 cycles, the cells were disassembled, then the Li electrode, the electrolyte, and the separator were replaced, and finally the cycling was continued under the same conditions. The cycling data of these experiments and pictures of the replaced separators are shown in Fig. 5. After replacement of these components, the $(\text{H}_2\text{AlO}^i\text{Bu})_2/\text{HF}$ coated NCM (160 to 166 mAh g^{-1} , +4.1%) as well as the pristine material (158 to 166 mAh g^{-1} , +5.4%) showed an increased practical specific charge. A comparison of the normalized potential profiles before and 5 cycles after the exchange of Li (Fig. 5b) shows that for both samples the overpotentials are reduced and this effect is much stronger for the pristine material. When looking at the replaced separators from both cell types (Figs. 5c and 5d), the separators from cells with uncoated NCM show brown residues, whereas the separators from the cells with coated NCM only show minor discoloration. In combination with the cycling data, these brown residues are a strong hint that there is a reaction of the cathode material with the electrolyte and/or with the electrolyte decomposition products, presumably from the Li counter electrode. From the slower fading of the coated cathodes as shown in Fig. 4, we conclude that both of the presented coatings seem to mitigate these side reactions.

Full-cell cycling of the coated (0.1 and 0.3 wt%) NCM cathode materials.—In order to eliminate the influence of the electrolyte decomposition products from the Li counter electrode, all materials were also tested in full cells with a graphite anode. The cycling was performed at both 25 °C and 45 °C. The additional higher temperature experiments were performed because faster degradation of the materials was expected. A different electrolyte in comparison to the half-cell experiments was used (LP47 vs LP572), the latter containing 2 wt% vinylene carbonate as additive needed to improve the cycling stability of the graphite anode.³⁷ The full-cell cycling data at a rate of 1 C at 45 °C for the pristine and coated samples ($(\text{H}_2\text{AlO}^i\text{Bu})_2$ and $(\text{H}_2\text{AlO}^i\text{Bu})_2 + 2 \text{HF}$, 0.3 and 0.1 wt% each) are shown in Fig. 6. Due to the formation of a stable SEI on the graphite negative electrode in full cells, the electrolyte is not constantly decomposed and therefore these decomposition products

cannot diffuse/migrate and react with the positive electrode (cf half-cells with Li anode, as discussed above). As a result, especially the cycling stability of the pristine NCM851005 is significantly improved in comparison to the half-cell experiments, and a capacity retention of 87% is measured after 300 cycles. For both 0.3 wt% coated samples the capacity retention is also improved in the full cells, but the $(\text{H}_2\text{AlO}^i\text{Bu})_2$ coated sample shows a slightly lower capacity retention (85%) than the pristine material whereas the one of the HF treated sample is identical (both 87%). Reducing the coating amount to 0.1 wt% leads to an increased capacity retention for the $(\text{H}_2\text{AlO}^i\text{Bu})_2$ coating (89%), but the subsequent HF treatment of this thin coating results in a slightly worse capacity retention of 86% after 300 cycles.

During the measurements of the internal resistance of the samples, which were performed at 25 °C, also specific charge data were obtained (Fig. 6b), which allow for comparison of the cycling performance of the samples at lower temperatures. At 25 °C all samples have lower capacity retentions after 300 cycles than at 45 °C. However, this effect is more pronounced for the pristine material with a decrease of the capacity retention to 78% (vs 87% at 45 °C). In contrast, the $(\text{H}_2\text{AlO}^i\text{Bu})_2$ coated materials are hardly affected by the lower temperature and reach capacity retentions of 85% (0.3 wt%, vs 86% at 45 °C) and 86% (0.1 wt%, vs 89% at 45 °C). The HF treated samples are more affected by the lower temperature and their capacity retentions decrease to 85% (0.3 wt%, vs 87% at 45 °C) and 81% (0.1 wt%, vs 86% at 45 °C). The trends of the capacity retention between the tested materials are reflected by the increase of the internal resistance shown in Table II. The pristine NCM, which has the lowest capacity retention at 25 °C of 78% after 300 cycles, has the highest resistance build-up of +351% after 280 cycles. The $(\text{H}_2\text{AlO}^i\text{Bu})_2$ coated samples show the best capacity retentions and the lowest resistance build-up of only +70% (0.3 wt%) and +115% (0.1 wt%) after 280 cycles, respectively. These observations correspond to the improved capacity retention of the coated materials in the half-cell tests at 25 °C shown in Fig. 4. The performance of the HF treated samples was between the pristine NCM and the $(\text{H}_2\text{AlO}^i\text{Bu})_2$ coated samples and so is their resistance build-up of +120% (0.3 wt%) and +274% (0.1 wt%).

The capacity retentions at the different cycling temperatures are quite different, and especially the pristine NCM seems to be more affected by temperature changes. We believe the better performance of the coated materials at 25 °C compared to the pristine NCM may be due to the good Li^+ ion conductivity of the LiAlO_2 and $\text{Li}[\text{AlO}(\text{OH})\text{F}]$ layers compared to the surface layer(s) on the pristine CAM. Raising the temperature to 45 °C increases the ion conductivity of NCM851005 and its surface layer(s) in general, thus reducing the differences in the achieved practical specific charges.

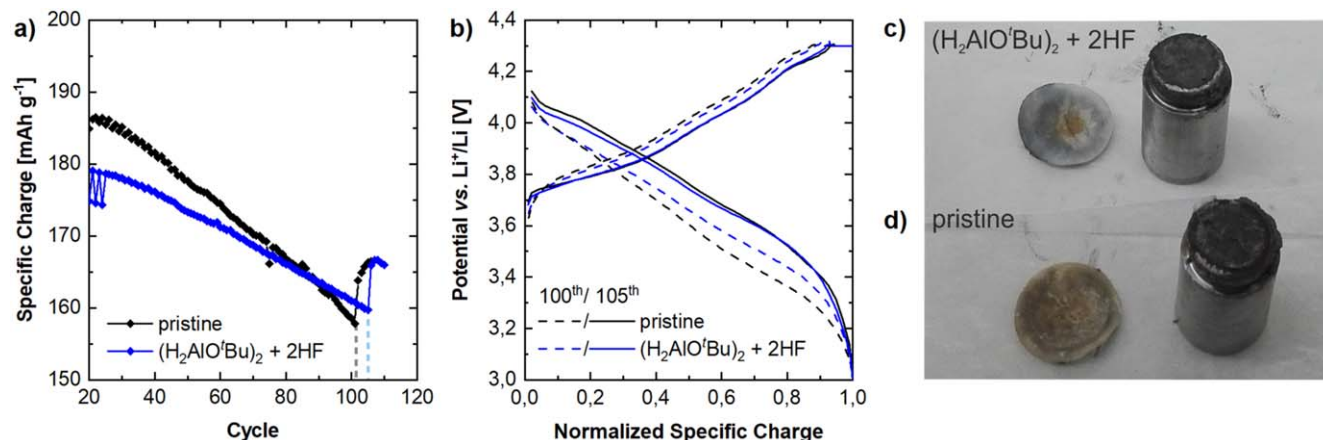


Figure 5. (a) Half-cell cycling data of $(\text{H}_2\text{AlO}^i\text{Bu})_2 + 2 \text{HF}$ coated (blue) and pristine (black) NCM851005, the vertical dashed line shows the replacement of the Li anode, electrolyte and separator. (b) Normalized specific charge for the 100th (dashed line) and 105th cycle (solid line; after replacement of Li, separator and electrolyte). (c) The cathode and separator of the half-cell containing the $(\text{H}_2\text{AlO}^i\text{Bu})_2$ (0.3 wt%) + 2 HF coated NCM851005 after 100 cycles. (d) The cathode and separator of the half-cell containing the pristine NCM851005 after 100 cycles.

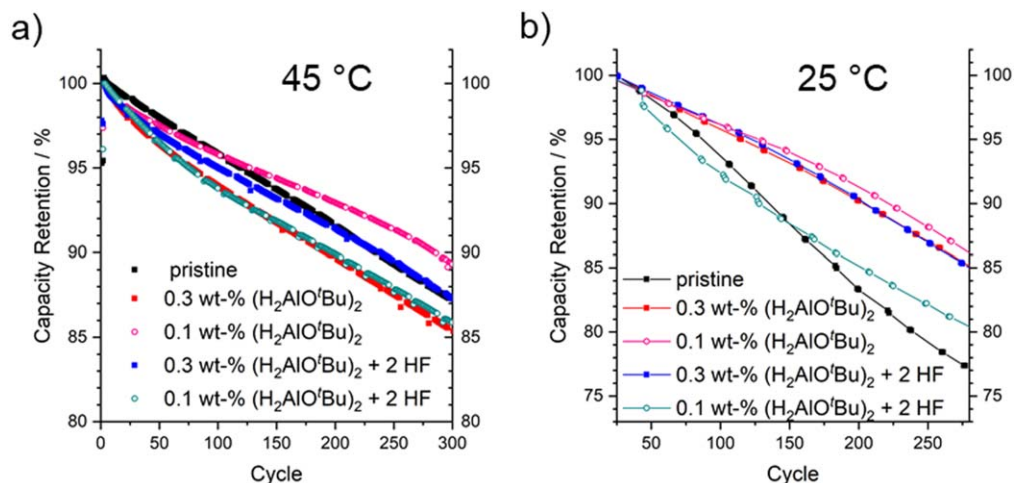


Figure 6. Discharge capacity retention during full-cell cycling of the pristine (black) and coated NCM851005 prior (red) and after treatment with HF (blue) using LP572 electrolyte. Cycling was performed at 1 C rate. The coating was performed using 0.3 wt% and 0.1 wt% (H₂AlO'Bu)₂, respectively. (a) Full-cell cycling data at 45 °C. The data from the resistance measurements performed at 25 °C have been removed (see experimental section). (b) Capacities obtained by the resistance measurements during full-cell cycling at 25 °C.

Discussion of the effects of the coatings applied.—Both the Al⁰@Al₂O₃/LiAlO₂ coating and the Al⁰/Li[AlO(OH)F] coating were shown to prevent reactions among the pristine NCM851005 and electrolyte decomposition products from Li anodes. We attribute this to the function of these coatings as “cathode SEI,” thus preventing side reactions of the CAM with the electrolyte and formation of other disadvantageous surface layers.^{33,38} Although these coatings slightly increase the initial resistance of the CAM, they mitigate the resistance build-up during prolonged cycling, presumably due to the presence of the conductive Al⁰ particles. This low resistance build-up might allow for long term cycling of the coated CAMs at higher rates compared to the pristine NCM851005.

A direct comparison between the Al⁰@Al₂O₃/LiAlO₂ and the Al⁰/Li[AlO(OH)F] coated CAMs using 0.3 wt% (H₂AlO'Bu)₂ reveals a relatively low performance of the former, by means of higher charge/lower discharge potential and worse cycling stability. One of the reasons for this could be that the Li[AlO(OH)F] layer may have a higher Li⁺ conductivity than LiAlO₂. The main reason, however, seems to be the formation of many ball-shaped Al⁰@Al₂O₃ particles upon coating of NCM851005 with (H₂AlO'Bu)₂. Although this results in a higher BET surface of the CAM (3.0 m² g⁻¹), the Al⁰@Al₂O₃ particles are not Li⁺ ion conductive. Hence, they hinder the transport of Li⁺ into and out of the CAM by reducing its Li⁺ conductive surface (Figs. 7a and 7b). Additionally, upon cycling, the Al₂O₃ can be lithiated to form lithium ion-conductive Li_xAl₂O₃, which would explain the high capacity fade upon the first cycles in the full-cell.³⁹

Treatment of the (H₂AlO'Bu)₂ coated CAM with HF not only transforms the LiAlO₂ layer into Li[AlO(OH)F] and LiF but it also heavily decreases the size and number of the Al⁰ containing

particles, as can be seen from the reduced BET specific surface area (0.5 m² g⁻¹), NMR spectra (lower Al⁰ content), and SEM images. The reduced amount of Al⁰@Al₂O₃ particles is a result of chemical etching of these particles with HF, leading to a more homogeneous distribution of the reaction products over the CAM's surface as can be seen from NMR spectra (same signal to noise ratio before and after HF treatment) and EDX elemental analysis (ESI, Fig. S-10). Also, SEM images show no additional particles next to the NCM (more SEM images in ESI, Figs. S-11 and S-12). Due to the fewer and smaller Al⁰@Al₂O₃ particles after treatment with HF the Li⁺ ion conductive surface layer is better accessible again and the cycling stability is improved (see Fig. 7c).

When reducing the amount of (H₂AlO'Bu)₂ used for both coatings from 0.3 to 0.1 wt%, the previous observations are inverted. Now the HF treated sample shows a significantly decreased capacity retention at 25 °C compared to the thick coating (0.3 wt%), while it is increased for the (H₂AlO'Bu)₂ coating. The latter coating probably contains less Al⁰@Al₂O₃ particles, which are also smaller, when using 0.1 wt% instead of 0.3 wt% (H₂AlO'Bu)₂, thus increasing the cycling performance while only slightly increasing resistance build-up (+70% vs +115% after 280 cycles). Since the thinner coating (0.1 wt%) contains less Al⁰ than the thick coating, subsequent treatment with HF reduces it even further, likely to a level too low to have significant impact on the NCM's electrical conductivity. Thus, the resistance build-up is heavily increased by the HF treatment from +115% to +274% after 280 cycles. The newly formed “Li[AlO(OH)F]” layer doesn't seem to improve the NCM's cycling stability with the same efficiency as LiAlO₂ (Fig. 6). Therefore, it seems that the HF treatment of the thick (0.3 wt%) Al⁰@Al₂O₃ coating only improved its performance due to a decrease of the Al⁰@Al₂O₃

Table II. Initial half-cell resistance and relative resistance (discharge capacity retention) upon long-term cycling at 45 °C of the pristine and coated NCM851005. Relative resistances were obtained at 25 °C Coating was performed using 0.3 and 0.1 wt% (H₂AlO'Bu)₂, respectively.

Cycle no.	Half-cell resistance/Ω cm ²	Relative resistance (discharge capacity retention)/%			
		50	100	200	300 ^{a)}
pristine	53.3	158 (98)	231 (96)	376 (91)	451 (87)
0.3 wt% (H ₂ AlO'Bu) ₂	57.0	111 (96)	121 (94)	145 (90)	170 (85)
0.1 wt% (H ₂ AlO'Bu) ₂	44.4	119 (98)	161 (96)	178 (93)	215 (89)
0.3 wt% (H ₂ AlO'Bu) ₂ + 2 HF	58.6	118 (97)	137 (95)	180 (91)	220 (87)
0.1 wt% (H ₂ AlO'Bu) ₂ + 2 HF	63.9	176 (97)	237 (94)	316 (90)	374 (86)

a) Resistances were obtained after 280 cycles.

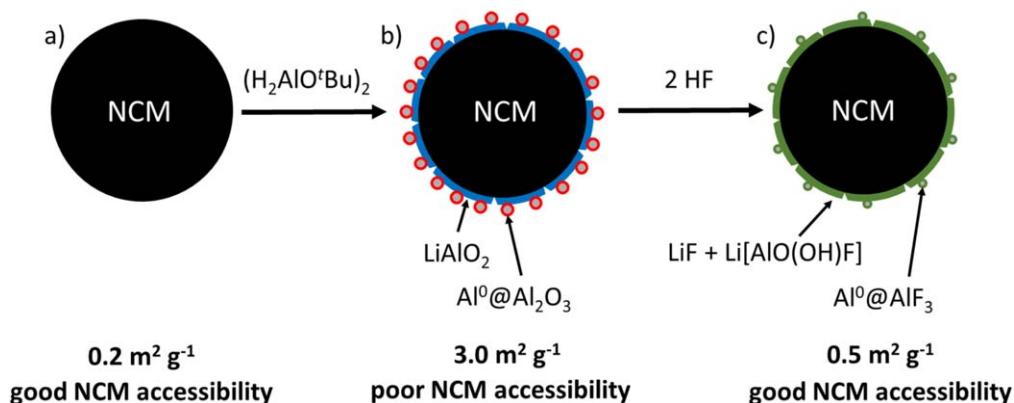


Figure 7. Schematic representation of the influence of the (H₂AlO'Bu)₂ coating (0.3 wt%) on the accessibility of the NCM surface. (a) Li ion transport into uncoated NCM is unhindered. (b) Coating of NCM851005 with (H₂AlO'Bu)₂ leads to formation of many Al⁰@Al₂O₃ particles. These decrease the surface of the Li ion conductive LiAlO₂ layer, thus hindering Li⁺ transport into and out of the NCM. (c) Treatment of the (H₂AlO'Bu)₂ coated NCM with 2 eq. HF decreases the size and number of the Al⁰@Al₂O₃ particles. Additionally, the Al₂O₃ layer is replaced by a thin "AlF₃" layer (see discussion below).

particles and not because of the Li⁺ ion conductivity of the "Li[AlO(OH)F]" layer. As a result, the optimization of the mass of (H₂AlO'Bu)₂ seems to be more reasonable than its treatment with HF (which basically has the same effect like a thinner coating).

Conclusion

The treatment of NCM851005 with 0.1 and 0.3 wt% (H₂AlO'Bu)₂, respectively, by a CVD-like batch process was shown to form a LiAlO₂ coating with inhomogeneously distributed Al⁰@Al₂O₃ particles. Electrochemical results show a reduced practical specific charge of the CAM after the coating with 0.3 wt% (H₂AlO'Bu)₂, probably a result of the bad accessibility of the CAM's surface for the Li⁺ ions. However, the coated NCM shows a significantly lower resistance build-up of only +70% after 280 cycles at 1 C cycling rate. Additionally, the coating increases the cycling stability of the CAM in the half-cell due to prevention of side reactions at the CAM's surface, initiated by the Li counter electrode. Reduction of the coating mass from 0.3 to 0.1 wt% slightly increased the resistance build-up to +115% after 280 cycles, but increased the capacity retention above the pristine material's (89% vs 87% after 300 cycles at 45 °C).

Treatment of the (H₂AlO'Bu)₂ coated (0.3 wt%) NCM851005 with 2 equiv. of anhydrous HF gas in respect to (H₂AlO'Bu)₂ changed the morphology of the coating to a more homogeneous layer with much less Al⁰ containing particles. Although electrochemical measurements in full-cells show a similar capacity as for the (H₂AlO'Bu)₂ treated NCM, the treated material shows an increased cycling stability both in the half and full-cells, which exceeds the stability of the pristine NCM. After the HF treatment the resistance build-up is slightly increased to +120% after 280 cycles at 1 C cycling rate but this is still much lower than for the uncoated sample (+351%). In contrast, treatment of the thinner coating (0.1 wt% (H₂AlO'Bu)₂) with HF decreased the performance of the initially coated NCM in all respects. Apparently, the treatment of the Al⁰/Al₂O₃ coated NCM851005 with HF increases its resistance build-up and also reduces the amount and size of Al⁰ particles. Therefore, we believe that the electric conductivity of the Al⁰ particles is of advantage for lowering the resistance build-up. As a conclusion it seems the HF treatment has the same effect like using less (H₂AlO'Bu)₂ for the coating, thus making it unnecessary.

We believe that especially the LiAlO₂/Al⁰@Al₂O₃ coating should be further investigated and optimized, as it can be achieved by a one-step procedure, independent of the layer thickness. In contrast, an ALD coating requires several steps per layer. Especially the coating of NCM851005 with only 0.1 wt% (H₂AlO'Bu)₂ improved its cycling stability, initial resistance, resistance build-up

and suppresses side reactions with the electrolyte at the same time, which should be beneficial in all battery applications.

Acknowledgment

This work was supported by the Albert-Ludwigs-Universität Freiburg, the Paul-Scherrer-Institute, and the BASF SE. We would like to thank Victoria Davis and Max Schmucker for the measurement of the EDX spectra.

References

1. F. A. Susai et al., *Adv. Mater.*, e1801348 (2018).
2. B. Han, T. Paulauskas, B. Key, C. Peebles, J. S. Park, R. F. Klie, J. T. Vaughey, and F. Dogan, *ACS Appl. Mater. Interfaces*, **9**, 14769 (2017).
3. K. M. Shaju, G. V. Subba Rao, and B. V. R. Chowdari, *Electrochim. Acta*, **48**, 145 (2002).
4. S.-K. Jung, H. Gwon, J. Hong, K.-Y. Park, D.-H. Seo, H. Kim, J. Hyun, W. Yang, and K. Kang, *Adv. Energy Mater.*, **4**, 1300787 (2014).
5. Z. Liu, A. Yu, and J. Y. Lee, *J. Power Sources*, **81-82**, 416 (1999).
6. J. Xu, F. Lin, M. M. Doeff, and W. Tong, *J. Mater. Chem. A*, **5**, 874 (2017).
7. F. Schipper, E. M. Erickson, C. Erk, J.-Y. Shin, F. F. Chesneau, and D. Aurbach, *J. Electrochem. Soc.*, **164**, A6220 (2017).
8. W. Liu, P. Oh, X. Liu, M.-J. Lee, W. Cho, S. Chae, Y. Kim, and J. Cho, *Angew. Chem. Int. Ed.*, **54**, 4440 (2015).
9. R. V. Moshchev, P. Zlatilova, V. Manev, and A. Sato, *J. Power Sources*, **54**, 329 (1995).
10. S.-M. Bak, E. Hu, Y. Zhou, X. Yu, S. D. Senanayake, S.-J. Cho, K.-B. Kim, K. Y. Chung, X.-Q. Yang, and K.-W. Nam, *ACS Appl. Mater. Interfaces*, **6**, 22594 (2014).
11. X. Zhang, I. Belharouak, L. Li, Y. Lei, J. W. Elam, A. Nie, X. Chen, R. S. Yassar, and R. L. Axelbaum, *Adv. Energy Mater.*, **3**, 1299 (2013).
12. F. Schipper et al., *Adv. Energy Mater.*, **8**, 1701682 (2018).
13. T. Zhao, S. Chen, R. Chen, L. Li, X. Zhang, M. Xie, and F. Wu, *ACS Appl. Mater. Interfaces*, **6**, 21711 (2014).
14. F. Amalraj et al., *J. Electrochem. Soc.*, **160**, A2220 (2013).
15. O. Srur-Lavi, V. Miikkulainen, B. Markovsky, J. Grinblat, M. Talianker, Y. Flegler, G. Cohen-Taguri, A. Mor, Y. Tal-Yosef, and D. Aurbach, *J. Electrochem. Soc.*, **164**, A3266 (2017).
16. J. Liu, B. Reeja-Jayan, and A. Manthiram, *J. Phys. Chem. C*, **114**, 9528 (2010).
17. Y. S. Jung, A. S. Cavanagh, A. C. Dillon, M. D. Groner, S. M. George, and S.-H. Lee, *J. Electrochem. Soc.*, **157**, A75 (2010).
18. M. Veith, S. Faber, H. Wolfanger, and V. Huch, *Chem. Ber.*, **129**, 381 (1996).
19. M. Veith, J. Lee, M. Martínez Miró, C. K. Akkan, C. Dufoux, and O. C. Aktas, *Chem. Soc. Rev.*, **41**, 5117 (2012).
20. S. Liu, U. Fookan, C. M. Burba, M. A. Eastman, and R. J. Wehmschulte, *Chem. Mater.*, **15**, 2803 (2003).
21. M. Veith, K. Andres, Stefan Faber, J. Blin, M. Zimmer, Y. Wolf, H. Schnöckel, R. Köppe, R. de Masi, and S. Hüfner, *Eur. J. Inorg. Chem.*, **2003**, 4387 (2003).
22. Y. Dong, M. Burkhart, M. Veith, and M. Springborg, *J. Phys. Chem. B*, **109**, 22820 (2005).
23. E. R. Andrew, W. S. Hinshaw, and R. S. Tiffen, *J. Magn. Reson.*, **15**, 191 (1974).
24. H.-S. Kim, Y. Kim, S.-I. Kim, and S. W. Martin, *J. Power Sources*, **161**, 623 (2006).
25. P. J. Chupas, D. R. Corbin, V. N. M. Rao, J. C. Hanson, and C. P. Grey, *J. Phys. Chem. B*, **107**, 8327 (2003).

26. P. J. Chupas and C. P. Grey, *J. Catal.*, **224**, 69 (2004).
27. F. Šimko, A. Rakhmatullin, P. Florian, M. Kontrik, M. Korenko, Z. Netroivá, V. Danielik, and C. Bessada, *Inorg. Chem.*, **56**, 13349 (2017).
28. D. Müller and U. Bentrup, *Z. Anorg. Allg. Chem.*, **575**, 17 (1989).
29. C. Bessada and E. M. Anghel, *Inorg. Chem.*, **42**, 3884 (2003).
30. L.-S. Du, A. Samoson, T. Tuhern, and C. P. Grey, *Chem. Mater.*, **12**, 3611 (2000).
31. J. F. Moulder and J. Chastain, in *Handbook of X-ray Photoelectron Spectroscopy: A Reference Book of Standard Spectra for Identification and Interpretation of XPS Data* (Perkin-Elmer Corporation Physical Electronics Division, Eden Prairie) (1992).
32. H. Younan, *13th International Symposium on the Physical and Failure Analysis of Integrated Circuits, [3–7 July 2006, Singapore]*(IEEE Service Center, Piscataway, NJ) p. 214 (2006).
33. A. M. Andersson, D. P. Abraham, R. Haasch, S. MacLaren, J. Liu, and K. Amine, *J. Electrochem. Soc.*, **149**, A1358 (2002).
34. K. Edström, T. Gustafsson, and J. O. Thomas, *Electrochim. Acta*, **50**, 397 (2004).
35. J. M. Paulsen, H.-K. Park, and Y. H. Kwon, "Process of making cathode material containing Ni-based lithium transition metal oxide." US Pat., US8574541 (B2) (2013).
36. J. M. Paulsen and Y. Kim, "High Nickel Cathode Material Having Low Soluble Base Content." US Pat. US054495 (A1) (2014).
37. D. Aurbach, K. Gamolsky, B. Markovsky, Y. Gofer, M. Schmidt, and U. Heider, *Electrochim. Acta*, **47**, 1423 (2002).
38. D. Aurbach, *J. Power Sources*, **119–121**, 497 (2003).
39. S. C. Jung and Y.-K. Han, *J. Phys. Chem. Lett.*, **4**, 2681 (2013).